A 1.05 $M_\odot$ COMPANION TO PSR J2222−0137: THE COOLEST KNOWN WHITE DWARF?

David L. Kaplan[1], Jason Boyles[2,3], Bart H. Dunlap[4], Shriharsh P. Tendulkar[5], Adam T. Deller[6],
Scott M. Ransom[7], Maura A. McLaughlin[2,9], Duncan R. Lorimer[2,9], and Ingrid H. Stairs[8]

[1] Department of Physics, University of Wisconsin-Milwaukee, 1900 East Kenwood Boulevard, Milwaukee, WI 53211, USA; kaplan@uwm.edu
[2] Department of Physics and Astronomy, West Virginia University, White Hall, Box 6315, Morgantown, WV 26506-6315, USA
[3] Physics and Astronomy Department, Western Kentucky University, 1906 College Heights Boulevard #11077, Bowling Green, KY 42101-1077, USA
[4] Department of Physics and Astronomy, University of North Carolina, Chapel Hill, NC 27599-3255, USA
[5] Space Radiation Laboratory, California Institute of Technology, 1200 East California Boulevard, MC 249-17, Pasadena, CA 91125, USA
[6] ASTRON, P.O. Box 2, 7990 AA Dwingeloo, The Netherlands
[7] National Radio Astronomy Observatory, 520 Edgemont Road, Charlottesville, VA 22903-2475, USA
[8] Department of Physics and Astronomy, University of British Columbia, 6224 Agricultural Road, Vancouver, British Columbia V6T 1Z1, Canada

ABSTRACT

The recycled pulsar PSR J2222−0137 is one of the closest known neutron stars (NSs) with a parallax distance of $267^{+1.2}_{-0.9}$ pc and an edge-on orbit. We measure the Shapiro delay in the system through pulsar timing with the Green Bank Telescope, deriving a low pulsar mass ($1.20 \pm 0.14\ M_\odot$) and a high companion mass ($1.05 \pm 0.06\ M_\odot$) consistent with either a low-mass NS or a high-mass white dwarf. We can largely reject the NS hypothesis on the basis of the system's extremely low eccentricity (3×10^{-4})—too low to have been the product of two supernovae under normal circumstances. However, despite deep optical and near-infrared searches with Southern Astrophysical Research and the Keck telescopes we have not discovered the optical counterpart of the system. This is consistent with the white dwarf hypothesis only if the effective temperature is <3000 K, a limit that is robust to distance, mass, and atmosphere uncertainties. This would make the companion to PSR J2222−0137 one of the coolest white dwarfs ever observed. For the implied age to be consistent with the age of the Milky Way requires the white dwarf to have already crystallized and entered the faster Debye-cooling regime.

Key words: binaries: general – pulsars: individual (PSR J2222-0137) – stars: distances –
stars: fundamental parameters

Online-only material: color figures

1. INTRODUCTION

PSR J2222−0137 (hereafter PSR J2222) is a 33 ms radio pulsar discovered in the Green Bank Telescope (GBT) 350 MHz drift-scan pulsar survey (Boyles et al. 2013). With a dispersion measure of 3.27 pc cm^{-3}, it appeared to be one of the closest pulsars to the Earth. Further observations showed PSR J2222 was in a binary system with an orbital period of 2.45 days and a minimum companion mass of about 1 $M_\odot$. This sort of system straddles the line between potential companion types. It could be a double-neutron star (DNS), of which there are only roughly 12 and whose study is crucial to understanding the formation of sources of kilohertz gravitational waves (e.g., Kim et al. 2003) and testing general relativity (e.g., Stairs 2010). Or, it could be a pulsar with a massive white dwarf companion—a so-called "intermediate-mass binary pulsar" (IMBP)—that descended from a binary with a more massive companion than in traditional systems with pulsars and low-mass white dwarfs (van den Heuvel 2004; Tauris et al. 2000, 2011, 2012). IMBP systems are rare, with fewer than 20 known, and massive white dwarfs are themselves rare, with fewer than 8% of the white dwarfs (WDs) from optical surveys having masses above 0.9 $M_\odot$ (Gianninas et al. 2011). Understanding the formation and evolution of IMBP systems provides a crucial piece in our understanding of binary evolution and pulsar recycling, and helps delineate evolutionary paths between low-mass NSs and high-mass white dwarfs (Tauris 2011).

Deller et al. (2013) used very long baseline interferometry astrometry to measure the parallax of PSR J2222 with exquisite

precision. They find a distance of $267^{+1.2}_{-0.9}$ pc (it is the second closest binary pulsar system and one of the closest NSs of any type). The astrometric data also suggested an edge-on orbit, opening up the possibility of a measurement of the Shapiro delay (Shapiro 1964), which gives two post-Keplerian (Lorimer & Kramer 2012) parameters for the system and hence determines the component masses (e.g., Demorest et al. 2010). Here we present the detailed timing analysis of the PSR J2222 system, including the measurement of the Shapiro delay and the determination of the masses (Section 2.1). We then present deep optical and near-infrared searches for the companion to PSR J2222 (Section 2.2), which we use to constrain models of its formation and evolution (Section 3). We find that the system almost certainly must be an IMBP system, but that we do not detect the companion, constraining it to be one of the coolest white dwarfs ever observed. Unlike some sources where temperature inferences are highly dependent on white dwarf model atmospheres (e.g., Gates et al. 2004), this measurement is robust, given the small uncertainties on the mass and (especially) distance. We conclude in Section 4.

2. OBSERVATIONS AND ANALYSIS

2.1. Radio Observations

Radio observations of PSR J2222 to measure the Shapiro delay occurred in the last week of 2011 May with the 100 m Robert C. Byrd GBT.[10] We had a 6 hr observation taken around

---

[9] Also adjunct at National Radio Astronomy Observatory, Green Bank, WV 24944, USA.

[10] The Robert C. Byrd Green Bank Telescope (GBT) is operated by the National Radio Astronomy Observatory which is a facility of the U.S. National Science Foundation operated under cooperative agreement by Associated Universities, Inc.
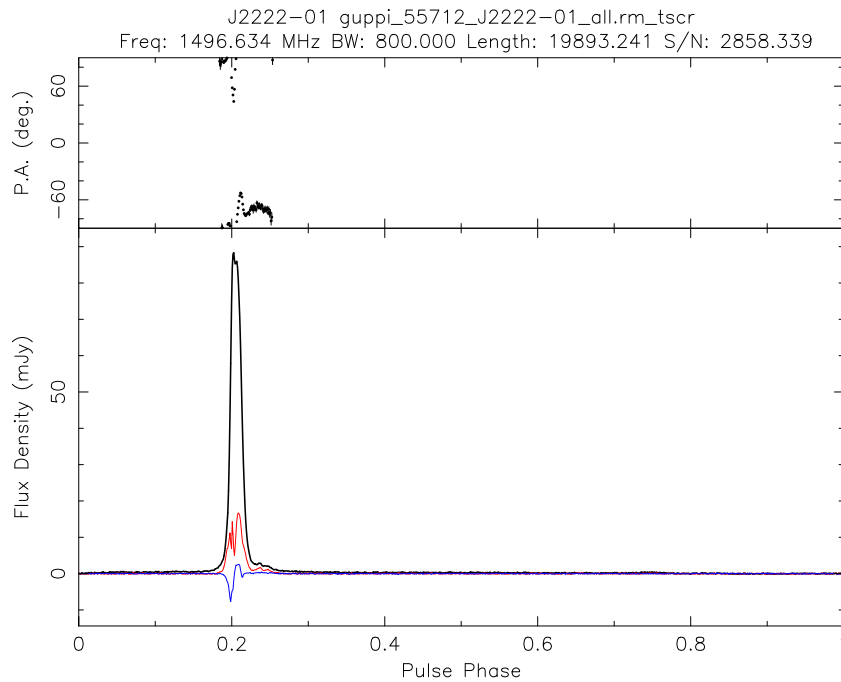
Figure 1. Pulse profile of PSR J2222 from the GUPPI observation covering conjunction. In the lower panel, black is the total intensity, red is linear polarization, and blue is circular polarization (Stokes *V*). The position angle of the linear polarization is given in the upper panel. As is the case with most MSPs, the polarization position angle variations do not permit a rotating vector model fit, so we cannot constrain the emission geometry.

(A color version of this figure is available in the online journal.)

superior conjunction of the binary system augmented by five 2 hr observations at each of the other five Shapiro extrema, all using the Green Bank Ultimate Pulsar Processing Instrument (GUPPI; DuPlain et al. 2008). The 800 MHz of bandwidth centered at 1500 MHz in two orthogonal polarizations was separated into 512 Nyquist-sampled frequency channels of width 1.5625 MHz via a polyphase filter bank. These channels, sampled at 8 bits, provided full polarization information and an effective time resolution of 0.64 μs. Each channel was coherently dedispersed at the nominal dispersion measure of the pulsar (3.27761 pc cm^{-3} at the time, although we later refined this measurement). Each observing session was broken into 30 minute observations of PSR J2222 separated by 60 s calibration scans of the extragalactic radio source 3C 190. The calibration scans were taken in the same mode as the pulsar observations, but also included a 25 Hz noise diode inserted into the receiver.

Data reduction was performed using the PSRCHIVE package (Hotan et al. 2004). Flux calibration used the on- and off-source scans of 3C 190. This was followed by removal of radio frequency interference by the psrzap utility. The calibrated pulse profile determined from the long observation covering conjunction is given in Figure 1. The data were aligned in time using the best ephemeris (below), divided into 16 frequency channels, and refit for dispersion measure and rotation measure using a bootstrap error analysis. We found that the period-averaged flux density varied by a factor of a few over the course of long observations due to scintillation, with an average of 1–2 mJy at 1500 MHz. Individual times of arrival (TOAs) were measured from the folded total-intensity profiles using the frequency domain algorithm in PSRCHIVE (Taylor 1992). A template was created by fitting three Gaussians to the summed pulse profile. From these Gaussian components, we created a noise-free template with the phase of the fundamental component in the frequency domain rotated to zero. The

observations were divided into two minute segments, with one TOA measured for each segment. Note that since interstellar scintillation caused the flux to vary considerably, there was a proportional change in the TOA precision that varied over the data set.

These data were combined with previous data taken for the discovery observations of PSR J2222 (Boyles et al. 2013) to produce a timing model. We used the "DD" model (Damour & Deruelle 1985, 1986) in TEMPO,[11] which incorporates the Shapiro delay. The astrometric data for this model were taken from Deller et al. (2013), and we used the DE421 JPL ephemeris (Folkner et al. 2009). Timing fits with no Shapiro delay were statistically unacceptable, with an rms residual of 9.3 μs ($\chi^2 = 4539.4$ for 931 degrees of freedom), and a clear Shapiro delay signature was obvious in the residuals (Figure 2). With the Shapiro delay included in the fit the rms residual was 4.2 μs ($\chi^2 = 930$ for 929 degrees of freedom), with no obvious remaining structure in the residuals (varying the astrometric parameters within the uncertainties from Deller et al. 2013 changed the timing results by $\ll 1\sigma$). The Shapiro delay determines the inclination of the orbit and the companion mass; this is then combined with the binary mass function to determine the pulsar's mass. Due to the combination of several different and much less precise observing modes from earlier monitoring with the high-precision Shapiro delay campaign, we estimated the timing parameters with a bootstrap error analysis. We give the full timing results, with 1σ error estimates from the bootstrap analysis, in Table 1.

Our data consist of high-quality coherently dedispersed data from an intensive one week campaign and a few other epochs. The remainder of the data were both less precise and less uniform, with a wider range of observation frequency and
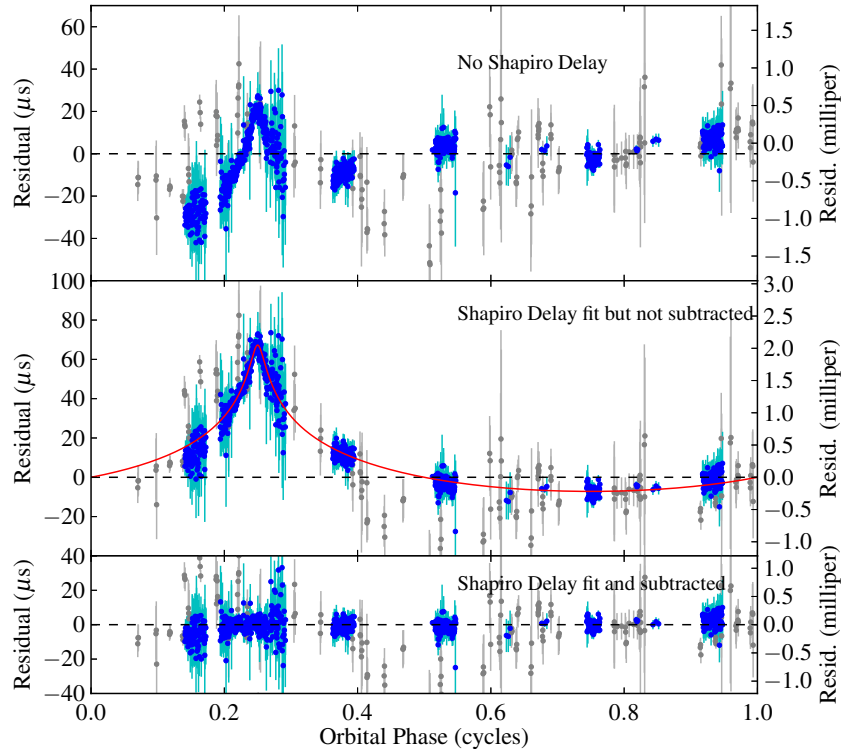
---

[11] http://tempo.sourceforge.net/.

Figure 2. Timing residuals for PSR J2222, using the new data from this paper (blue: MJD 55,600–55,921) and older data (gray), as a function of orbital phase (true anomaly plus longitude of periastron). Top: residuals computed from the best-fit model without Shapiro delay (the rms residual is 9.3 μs). Middle: residuals computed including Shapiro delay. The red curve is the best-fit Shapiro delay profile. Bottom: residuals computed relative to the best-fit model including Shapiro delay (the rms residual is 4.2 μs). Conjunction is at a phase of 0.25. In all panels the left axis shows the residuals in μs, while the right axis shows the residuals in milliperiods. Note the different y-axis scales.

(A color version of this figure is available in the online journal.)

instrumental setup. This makes it difficult (if not impossible) to robustly constrain long-term secular changes like periastron precession ($\dot{\omega}$; Lorimer & Kramer 2012). Nonetheless, we tried a fit with $\dot{\omega}$ fixed to the value predicted by general relativity ($\approx$0°.08 yr^{-1}). The resulting fit was good, with the rms decreasing to 3.8 μs. The pulsar and companion masses each increased by about 1σ compared to the values in Table 1. Given the small eccentricity and inhomogeneous data set with large gaps we do not believe that fitting for $\dot{\omega}$ is viable at this time, but encourage further long-term monitoring of this system to establish its secular behavior.

2.2. Optical/IR Observations

We observed the position of PSR J2222 at optical and near-infrared wavelengths, as listed in Table 2. The deepest Keck observations used the red side of the Low-Resolution Imaging Spectrometer (LRIS; Oke et al. 1995) on the 10 m Keck I telescope. The data were reduced using standard procedures in IRAF, subtracting the bias, dividing by flatfields, and combining the individual exposures. The seeing was about 0″.8 in the combined R image, and 0″.7 in the combined I image. We computed an astrometric solution fitting for a shift and separate scales and rotations along each axis (i.e., a six parameter fit) using 100 non-saturated stars identified from the Sloan Digital Sky Survey (SDSS) Data Release 10 (DR10; Ahn et al. 2014), giving rms residuals of 0″.2 in each coordinate. We did photometric calibration relative to SDSS photometry, identifying 23 well-detected, well-separated, non-saturated stars, and transforming from the SDSS filter set to Johnson–Cousins using the appropriate

transformation equations.[12] The zero-point uncertainty was <0.01 mag, although there are systematic uncertainties coming from our filter transformations. We see no object at the position of the pulsar (Figure 3); the closest object is about 2″ from the position of the pulsar (about 10σ away) and appears extended ($R = 23.1 \pm 0.1$ and statistical position uncertainties of $\pm$0″.3 in each coordinate). We determined the 3σ upper limits using sextractor (Bertin & Arnouts 1996) to determine the magnitude that gave a 0.3 mag uncertainty (verified with fake-star tests), which we give in Table 2.

We observed PSR J2222 in r-band with the Goodman Spectrograph (Clemens et al. 2004) on the 4.1 m Southern Astrophysical Research (SOAR) telescope over two nights in 2013 July. All exposures were dithered and binned by a factor of two in both dimensions. The frames were bias-subtracted and flattened with a dome flat. We then used a median of the data (having masked the scattered-light halos of three saturated stars) from the second night constructed without registration to create a sky flat, which we smoothed with a 20 × 20 pixel boxcar filter. This corrects for larger-scale brightness variations. Cosmic rays were interpolated on individual exposures using the lacosmic routine (van Dokkum 2001). The seeing varied considerably over the course of the observations, going from 1″.1 to 2″. We then shifted each exposure by an integer number of pixels for registration and summed them. The final summed image has an effective seeing of 1″.3 and a total exposure time of 2.6 hr. The photometric zero-point was again computed relative

---

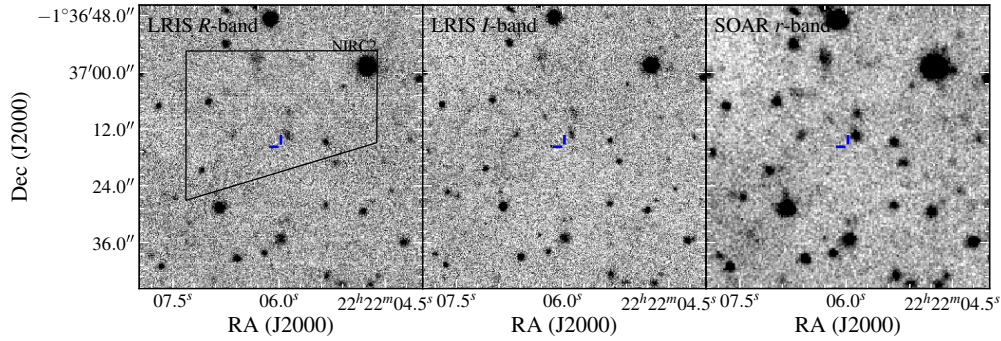[12] See http://www.sdss.org/dr5/algorithms/sdssUBVRITransform.html#Lupton2005.

Figure 3. Optical images of the field of PSR J2222: LRIS *R* band (left), LRIS *I* band (middle), and SOAR *r* band (right). The position of PSR J2222 is indicated with the ticks at the center, which begin 0″.5 from the pulsar (larger than the position uncertainty of the pulsar combined with the astrometric uncertainty of the image). North is up, east to the left, and the image is 1′ in size. On the *R*-band image we also indicate the field-of-view covered by our NIRC2 image, with the region masked apparent in the lower-right.

(A color version of this figure is available in the online journal.)

Table 1
Fitted and Derived Timing Parameters for PSR J2222−0137

Parameters	Value
Timing Parameters	
Spin period (s)	0.032817859053065(3)
Period derivative (s s^{-1})	5.865(7) × 10^{-20}
Dispersion measure (pc cm^{-3})	3.2842(6)
Rotation measure (rad m^{-2})	+2.6(1)
Reference epoch (MJD)	55743
Right ascension[b] (J2000)	22:22:05.969101(1)
Declination[b] (J2000)	−01:37:15.72441(4)
R.A. proper motion[b] (mas yr^{-1})	44.73(4)
Decl. proper motion[b] (mas yr^{-1})	−5.68(6)
Parallax[b] (mas)	3.742$^{+0.013}_{-0.016}$
Position epoch[b] (MJD)	55743
Span of timing sata (MJD)	55005–55922
Number of TOAs[a]	943
rms residual (μs)	4.2
Binary parameters[d]	
Orbital period (days)	2.4457599929(3)
Projected semi-major axis (lt-s)	10.8480276(12)
Epoch of periastron (MJD)	55742.13242(0)
Orbital eccentricity	3.8086(15) × 10^{-4}
Longitude of periastron (deg)	119.778(12)
Mass function ($M_\odot$)	0.22907971(8)
sin *i*	0.9985(3)
Companion mass ($M_\odot$)	1.05(6)
Derived parameters	
Distance[b] (pc)	267.3$^{+1.2}_{-0.9}$
Transverse velocity[b] (km s^{-1})	57.1$^{+0.3}_{-0.2}$
Orbital inclination *i* (deg)	86.8(4)
Shklovskii period derivative (s s^{-1})	4.33(5) × 10^{-20}
Intrinsic period derivative[c] (s s^{-1})	1.54(5) × 10^{-20}
Surface magnetic field[c] (10^9 G)	0.719
Spin-down luminosity[c] (10^{31} erg s^{-1})	1.72
Characteristic age[c] (Gyr)	33.8
Pulsar mass ($M_\odot$)	1.20(14)
Flux density at 1500 MHz (mJy)	1–2

Notes. Values in parentheses are uncertainties on the last digit. For the timing data derived here, the uncertainties were derived from a bootstrap analysis and are quoted at the 1σ level.
[a] During the initial timing observations we calculated a TOA every 10 minutes. During the new observations described here we calculated a TOA every two minutes.
[b] Values are from Deller et al. (2013) and were held fixed for the timing fit.
[c] Values are corrected for Shklovskii effect.
[d] We used the "DD" model (Damour & Deruelle 1985, 1986).

Table 2
Optical/Near-infrared Observations and Limiting Magnitudes

Instrument	Date	Filter	Exposure	Limiting Magnitude	
			(s)	Apparent[a]	Absolute[b]
SOAR/Goodman	2013 Jul 2	*r*	300 + 3 × 600	26.4[c]	19.2
SOAR/Goodman	2013 Jul 3	*r*	18 × 400		
Keck I/LRIS(red)	2013 Aug 4	*R*	2 × 300	26.3	19.1
Keck I/LRIS(red)	2013 Aug 4	*I*	2 × 300	26.0	18.9
Keck II/NIRC2	2013 Oct 12	*K′*	60 + 5 × 120	21.0	13.9

Notes.
[a] 3σ limiting magnitudes at the position of the pulsar.
[b] Absolute magnitude limits computed for a distance of 267 pc and an extinction of $A_V = 0.12$ mag.
[c] The two SOAR observations were combined.

to the SDSS DR10 data, using 31 stars. The astrometric solution was done using six 30 s exposures through http://astrometry.net (Lang et al. 2010). As with the Keck data, we see no object at the position of the pulsar (Figure 3) and give a 3σ upper limit in Table 2.

While they were taken through different filters and with very different instruments/resolutions, we tried combining the Keck *R*-band and SOAR *r*-band images using swarp (Bertin et al. 2002). We still see no source at the position of the pulsar. The data are sufficiently different that a limiting flux is difficult to compute, but it could be as much as 0.3 mag fainter than the limits in Table 2.

The near-infrared observations come from the NIRC2 camera[13] on the 10 m Keck II telescope, and used the Laser Guide Star Adaptive Optics (AO) system (van Dam et al. 2006). The data were taken through thin clouds and the AO corrections were not optimal, resulting in a delivered image quality of 0″.2 FWHM. The images were reduced using a custom pipeline implemented with python and pyraf using dark frames and dome-flats. A sky fringe frame was created by combining dithered images of multiple targets with the bright stars masked. We used SExtractor (Bertin & Arnouts 1996) for the preliminary detection and masking of stars. The fringe frame was subtracted from the flat-fielded data after being scaled to the appropriate sky background level. Before coadding the frames, each frame was corrected for optical distortion using a distortion solution

---

[13] The NIRC2 camera can be utilized in three different magnification modes. We used the "wide" camera with a 40″ square field of view.

measured for NIRC2.[14] A faint glare has been visible in the lower right (southwest) corner of the NIRC2 wide camera images starting in 2009 August. The shape and amplitude of the glare vary with telescope orientation, resisting correction through surface fitting or modeling. Instead we masked the glare using a triangular region. There was no independent photometric calibration that night, and only a single star is visible on the co-added image. To determine a photometric zero-point, we used photometry for that star from the SDSS DR10. We then employed the empirical main-sequence color relations from Covey et al. (2007), inferring the $z - K_s$ color from the observed $g - i$ color (we ignore differences between K_s and K' filters). For this star (SDSS J222204.76−013658.9) we infer a spectral type of K2.5 and predict $K_s = 16.9$. We expect zero-point uncertainties of ±0.2 mag or so based on comparison of the other SDSS colors to those predicted using Covey et al. (2007). Again, we see no object at the position of the pulsar, and give 3σ upper limits in Table 2.

3. DISCUSSION

3.1. A Low-mass Neutron Star?

Since we do not detect the optical counterpart of the companion, the first inference is that the companion could be a low-mass NS. It would be the lowest mass NS known (Lattimer 2012; Özel et al. 2012; Kiziltan et al. 2013), although it is only a roughly 2–3σ excursion from the mean of the companions in DNS systems (Özel et al. 2012; Kiziltan et al. 2013): rare, given the ≈10 DNS systems, but not impossible.

In that case, its eccentricity of 3.8×10^{-4} would be a factor of 200 lower than any other DNS system (PSR J1906+0746 has the lowest eccentricity of $e = 0.085$, although this may be an NS–WD system; Kasian 2012; van Leeuwen et al. 2014). In Figure 4, we show the eccentricity versus component masses for all DNS and NS–WD systems with well-determined masses. In fact, there are three NS–WD systems with higher eccentricities: PSR J1141−6545, which was likely not recycled (Kaspi et al. 2000); PSR J0337+1715, which has had its eccentricity increased by dynamical interactions (Ransom et al. 2014); and PSR J0621+1002 (likely an IMBP, with the eccentricity the result of unstable mass transfer; Phinney & Kulkarni 1994; Camilo et al. 2001).

The normal formation scenario for a DNS involves two core-collapse supernova explosions, with the eccentricity the result of the second explosion and its kick, and no final mass-transfer phase to circularize the orbit (e.g., Tauris & van den Heuvel 2006). In contrast, formation via an electron-capture supernova (ECS; Miyaji et al. 1980) could result in a significantly lower NS mass (Schwab et al. 2010; Ferdman et al. 2013) along with a lower supernova kick (Podsiadlowski et al. 2004; van den Heuvel 2004). PSR J2222 has a low transverse velocity (58 km s^{-1}), although higher than some systems thought to be the products of ECSs (given the age of the system, this velocity may be more related to motion in the Galactic potential than birth conditions). This may reflect the velocity dispersion of the progenitor systems. However, the contrast between PSR J2222 and other systems thought to be the results of ECSs (e.g., PSR J1906+0746 or PSR J0737−3039; Ferdman et al. 2013) is extreme, with the ratio of eccentricities above 200 as mentioned previously. In a scenario without a kick we can place an upper limit on the amount of material that could have been ejected
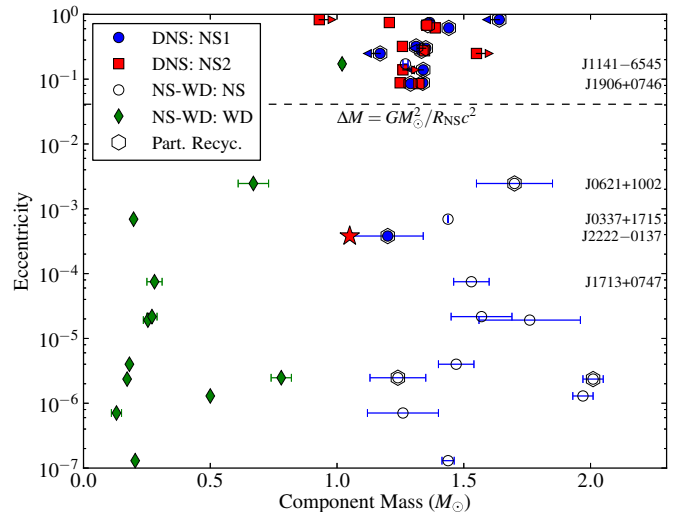

Figure 4. Mass vs. orbital eccentricity for DNS systems and NS–WD systems. The data are for those systems with well-determined (from radio timing and optical spectroscopy) masses from Ferdman et al. (2013) and Kiziltan et al. (2013), augmented by Keith et al. (2009), Lynch et al. (2012), Antoniadis et al. (2012), Antoniadis et al. (2013), and Ransom et al. (2014; inner companion only). For the DNS systems the primary (recycled) NS is the blue circle, while the secondary NS is the red square. For the NS–WD systems the NS is an open circle, while the WD is a green diamond. Those systems that are only partially recycled (with spin periods between 10 ms and 0.2 s) are indicated by hexagons. We exclude the NS–WD systems in globular clusters, where the eccentricity can be influenced by dynamical encounters. In some cases, the nature of the companion (WD vs. NS) is not clear, such as in PSR J1906+0746 (van Leeuwen et al. 2014) and PSR J2222 (the red star). Selected systems are labeled. The horizontal line is given by $e = \Delta M_c / (M_c + M_{\rm NS})$ (Bhattacharya & van den Heuvel 1991), with $\Delta M_c = GM_\odot^2 / R_{\rm NS} c^2$ the minimum change in binding energy needed to form an NS (Freire & Tauris 2014): all confirmed DNS systems are found above this line.

(A color version of this figure is available in the online journal.)

by the explosion to $(M_{\rm PSR} + M_c)e = 8 \times 10^{-4} M_\odot$ (with $M_{\rm psr}$ the pulsar mass and M_c the current companion mass; e.g., Bhattacharya & van den Heuvel 1991). This is a much tighter bound than in any of the other systems proposed for this mechanism, and difficult to reconcile with the change in binding energy needed to collapse to an NS $\sim GM_c^2 / R_c c^2 \approx 0.1 M_\odot$ (with $R_c \approx 15$ km for an NS), presumably released as neutrinos (e.g., Freire & Tauris 2014): this leads to the horizontal line in Figure 4, above which all confirmed DNS systems are found. In order to have a DNS system with such a low eccentricity, we need to invoke increasingly exotic (and perhaps implausible) evolutionary scenarios. For instance, if the system began as a hierarchical triple (Champion et al. 2008; Ransom et al. 2014; Tauris & van den Heuvel 2014), then the inner components could have formed a standard eccentric DNS system early on. Later evolution of the outer member could have led to a circumbinary accretion disk that would have worked to circularize the inner system, after which the outer object would have exploded or otherwise been ejected from the system.

3.2. An Intermediate-mass Binary Pulsar?

The other possible scenario is that the companion could be a massive WD, making the system an IMBP. Its orbital eccentricity is somewhat high compared to most low-mass binary pulsars of similar periods (based on Phinney 1992), but not nearly as high as a DNS, consistent with an IMBP classification (Camilo et al. 2001). It falls in the locus of other CO WDs in the "Corbet" (binary period versus spin period)

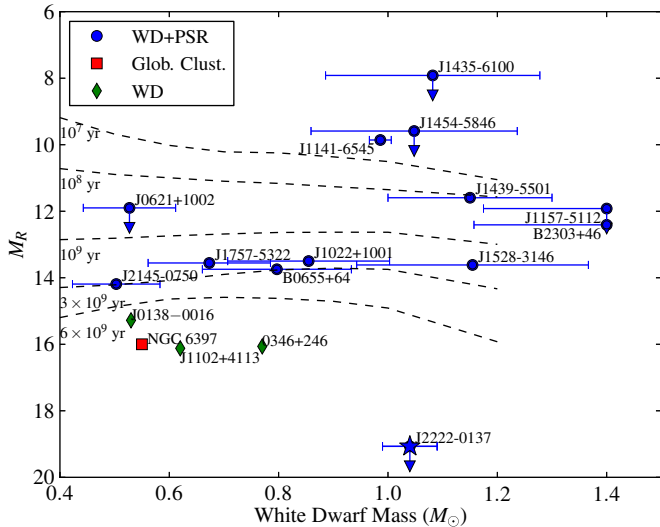[14] See http://www2.keck.hawaii.edu/inst/nirc2/dewarp.html.

Figure 5. Absolute R magnitude plotted against WD mass for massive and/or cool WDs. We show the IMBPs and massive WDs from van Kerkwijk et al. (2005) and Jacoby et al. (2006), with PSR J1141−6545 updated from Antoniadis et al. (2011) and PSR J1439−5501 from Pallanca et al. (2013). Data from bands other than R were converted to R using the photometry of Tremblay et al. (2011) and with extinctions from Drimmel et al. (2003) computed for the distances of the pulsars, except for updated extinctions for PSR J1439−5501 (Pallanca et al. 2013) and PSR B2303+46 (van Kerkwijk & Kulkarni 1999). All other pulsar data come from Manchester et al. (2005; ver. 1.48). Distances are from Cordes & Lazio (2002), except PSRs J1022+1001 and J2145−0750 (A. T. Deller et al. 2014, private communication), PSR J1141−6545 (Ord et al. 2002), and PSR J1439−5501 (Pallanca et al. 2013). When the inclination is not constrained, the point is at the median value (inclination of 60°) but a range is indicated by the error bars, and we allow a maximum companion mass of 1.4 $M_\odot$. We also show the approximate truncation of the WD cooling sequence from the halo globular cluster NGC 6397 (square; Richer et al. 2006; Hansen et al. 2007; Richer et al. 2013), as well as isolated cool halo WDs and the eclipsing ultra-cool WD SDSS J0138−0106 (diamonds; Kilic et al. 2012; Parsons et al. 2012). The dashed lines show contours of constant age for DA WDs based on Tremblay et al. (2011), with the ages listed at the left.

(A color version of this figure is available in the online journal.)

diagram in Tauris et al. (2012). The pulsar mass is lower than most pulsar–WD binaries, but is consistent with the short orbital-period IMBP discussed by Ferdman et al. (2010) which may indicate a similar formation mechanism involving a common envelope (Tauris & van den Heuvel 2006).

However, as a WD it would be extremely faint: far fainter than any of the optical companions to IMBPs currently known (van Kerkwijk et al. 2005; Jacoby et al. 2006; Pallanca et al. 2013) or indeed any WD companion to a millisecond pulsar (MSP) with a similar mass (Antoniadis et al. 2011); it is perhaps the faintest WD ever observed. With the apparent magnitude limits from Table 2, we can compute absolute magnitude limits in each band. We use the distance 267 ± 1 pc (Deller et al. 2013), and we estimate the extinction to be $A_V = 0.12$ mag from Drimmel et al. (2003). In terms of bolometric luminosity, the most constraining limit ends up coming from the R-band data, where we limit $M_R > 19.1$ (the r-band limit of $M_r > 19.2$ is very similar, given slight differences in bolometric correction). For comparison, the companion to PSR J1022+1001 with a median companion mass of 0.85 $M_\odot$ has $M_R \approx 14$ (Lundgren et al. 1996). In Figure 5, we plot the absolute magnitude against mass for pulsar+WD systems as well as select cool WDs with parallax distances: even compared to the observed truncation of the cooling sequence in old halo globular clusters like NGC 6397 (Richer et al. 2013) or M4 (Bedin et al. 2009), the putative companion is far fainter: at the distance of NGC 6397, our limit
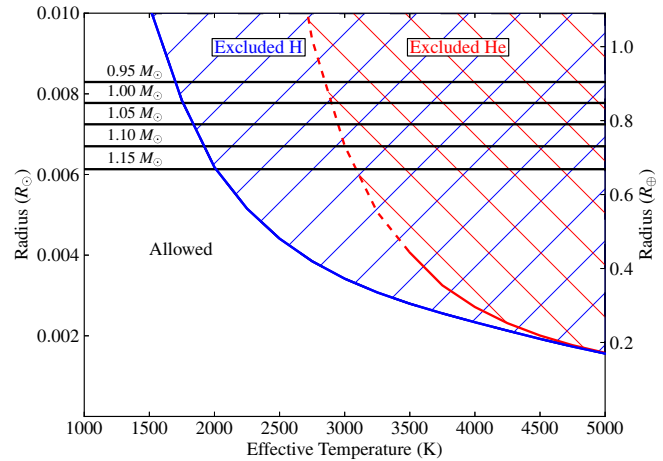

Figure 6. Constraints on the radius of any WD companion to PSR J2222, as a function of effective temperature. The blue-hatched region shows the excluded parameter space for an H atmosphere (DA) white dwarf based on our R-band photometry (the r-band limit of $M_r > 19.2$ is very similar, given slight differences in bolometric correction), where we have used the synthetic model for the 1.0 $M_\odot$ DA WD to compute bolometric corrections as a function of effective temperature. The red-hatched region shows the excluded parameter space for an He atmosphere (DB) white dwarf; we have extrapolated that model below 3500 K with a blackbody (dashed segment), which is appropriate given the uncertainties in the equation-of-state in this regime. The allowed radii should be compared with the radii of C/O WDs with masses from 0.95 $M_\odot$ to 1.15 $M_\odot$ (roughly our 2σ range from our mass measurements), shown by the horizontal lines.

(A color version of this figure is available in the online journal.)

of $M_R > 19.1$ translates to an apparent magnitude of $R > 31.6$, compared to $R \approx 29$, or $M_R \approx 16$ for the coolest WDs seen in NGC 6397. Some of the difference comes from the change in radius: a 1.0 $M_\odot$ WD has a radius about 65% of that of a typical 0.6 $M_\odot$ WD, leading to a 1 mag change in brightness at the same effective temperature. However, the difference in Figure 5 is more like 2.5 mag, so the companion to PSR J2222 must also be cooler than the known thick disk/halo WDs.

Beyond the absolute magnitude, which is directly computable from observable quantities, we can limit the radius/temperature of a putative WD by using our R-band absolute magnitude limit to constrain the bolometric luminosity. This is more compli-cated, as it involves atmosphere calculations in an uncertain and poorly tested regime, but it should be reasonably reliable. We use the synthetic photometry and evolutionary models from Tremblay et al. (2011) and Bergeron et al. (2011) for H and He atmospheres, respectively.[15] For isolated WDs pure He atmo-spheres can be largely excluded because of Bondi-Hoyle accre-tion from the ISM (Bergeron 2001), and even small amounts of hydrogen mixed into the helium can cause near-infrared flux deficiencies like pure hydrogen (see below; Bergeron & Leggett 2002). However, the binary orbit and MSP wind in this system could have inhibited such accretion and therefore a He atmo-sphere is possible. In any case, a pure He atmosphere will serve as a limiting case compared to the H models. These models are used to convert the absolute magnitude limits into tempera-ture limits, so for simplicity we use the 1.0 $M_\odot$ models (differ-ences in bolometric corrections as a function of mass are small, <0.05 mag).

The most constraining limit is again from the R-band data, where $M_R > 19.1$ implies $T_{\rm eff} < 1700$ K (see Figure 6) for an H atmosphere. The He-atmosphere models do not

---

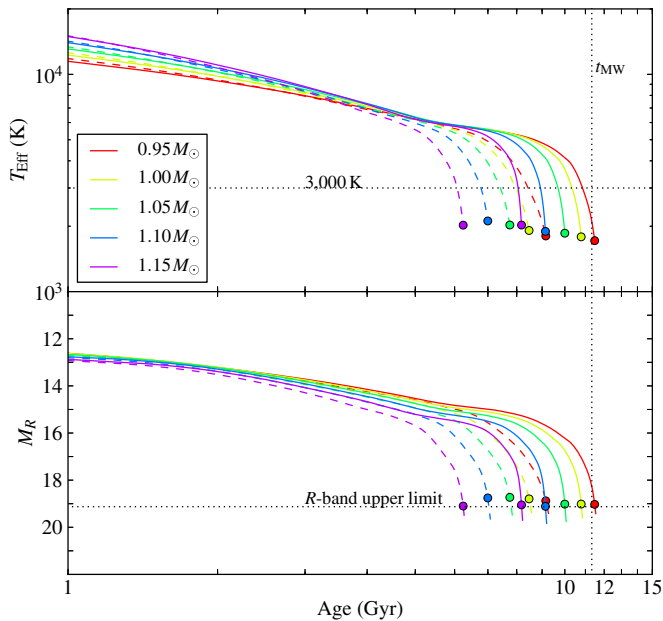[15] Also see http://www.astro.umontreal.ca/~bergeron/CoolingModels/.

Figure 7. Cooling of massive H-atmosphere CO WDs, based on the models of Bergeron et al. (2011; also see Kowalski & Saumon 2006; Holberg & Bergeron 2006; Tremblay et al. 2011). We show the effective temperature (top), and R-band (bottom) absolute magnitudes for ages of >1 Gyr. The models span the $\pm 2\sigma$ mass range of PSR J2222's companion, from $0.95\,M_\odot$ to $1.15\,M_\odot$, and include thin (hydrogen 10^{-10} by mass; dashed lines) and thick (hydrogen 10^{-4} by mass; solid lines) hydrogen atmospheres. The spin-down age of the pulsar τ_c is 34 Gyr and is far to the right. Instead, we show with a vertical dotted line the age of the Milky Way's inner halo (Kalirai 2012) as an upper bound to the age of any star not found in a globular cluster. The R-band upper limits are the horizontal dotted lines in the lower panel: in the top panel, the cooling curves stop when the implied R-band photometry reaches our upper limit (filled circles), which happens at an effective temperature of 2000–3000 K (3000 K is indicated by the dotted line in the top panel). To compute the synthetic photometry we have used the synthetic model for the $1.0\,M_\odot$ DA WD to compute bolometric corrections as a function of effective temperature, which we then applied to the cooling models.

(A color version of this figure is available in the online journal.)

extend to sufficiently cool temperatures but stop at $T_{\rm eff} = 3500$ K with $M_R = 17.7$. At lower temperatures the details of the atmospheric physics are rather uncertain, but a blackbody is likely an acceptable approximation (P. Bergeron 2014, private communication). With an He atmosphere an effective temperature <3000 K would be required (Figure 6). The H limits are more constraining since more of the flux appears in the optical regime rather than the near-infrared—a consequence of collisionally induced absorption by molecular H_2 (Bergeron et al. 1995; Hansen 1998). These limits change slightly with mass given the small but finite mass uncertainties, since the radius would change with mass: going to the $1.2\,M_\odot$ H model we can constrain $T_{\rm eff} < 2100$ K (at our nominal mass of $1.05\,M_\odot$ the radius of a C/O WD is about $0.0073\,R_\odot$, and it scales as $R \propto M^{-1.6}$). As inferred from Figure 5, the companion to PSR J2222 would be far cooler than any known WD from other surveys (e.g., Kilic et al. 2012; Catalán et al. 2012, 2013), where the coolest objects tend to have $T_{\rm eff} \approx 3800$ K.

However, we cannot exclude such a very cool WD on age grounds. WD cooling curves, which start out having more massive objects warmer at the same age, eventually cross to have more massive objects cooler at the same age (Figure 7; this is also visible in Figure 5). This is because massive WDs crystallize earlier, at a higher $T_{\rm eff}$ (but at a similar internal temperature), at which point the faster Debye cooling takes

over (Mestel & Ruderman 1967; van Horn 1968; Chabrier et al. 2000). Cooling ages for these models may not be reliable, as the impacts of state changes, sedimentation, and chemical processes are not precisely known, and the atmospheres are not trivial to calculate (Montgomery et al. 1999; Chabrier et al. 2000; Althaus et al. 2007; Salaris et al. 2010; Tremblay et al. 2011). But we believe conservatively that the cooling age is close to 10 Gyr, almost certainly >8 Gyr. In Figure 7, we show example cooling curves, computed for thin and thick DA atmospheres and C/O WDs (likely irradiation is a negligible perturbation to the WDs surface temperature, given the measured spin-down luminosity of the pulsar). For the model closest to the best-fit mass of PSR J2222 we would infer that the true age is near 9 Gyr, with the possible range from 6–12 Gyr. The upper limit provided by the pulsar's characteristic spin-down age (34 Gyr after correction for the Shklovskii effect; Shklovskii 1970) is not constraining; the assumption that the pulsar's initial spin period is much shorter than the current spin period is clearly not valid. Instead, we take as our upper limit to the age that of the Milky Way's halo (11.4 ± 0.7 Gyr; Kalirai 2012) minus the ≈ 70 Myr required for the main-sequence lifetime of a $\approx 6\,M_\odot$ progenitor (Koester & Reimers 1996; Williams et al. 2009), although this does not really exclude any models. Such an age would, however, imply a lower limit to the (re-)birth period of about 25 ms, assuming spin-down with a braking index $n = 3$ (magnetic dipole radiation). We note that the cooling models in Figure 7 may not be the only solution for this progenitor: changing the WD composition (likely it is below the transition to O/Ne/Mg WDs based on Nomoto 1984; Iben & Tutukov 1985, although binary evolution could change that; also see Lazarus et al. 2014) or atmosphere (helium, carbon, etc) could lead to different solutions, and to draw robust conclusions we need to explore a wider range of models with better observational constraints. There are also considerable complications and uncertainties in models for these temperatures: for instance, the models of Salaris et al. (2010; the BaSTI database) give rather different ages as $T_{\rm eff}$ never drops below 4000 K for $1.0\,M_\odot$ models, even for ages of >14 Gyr, while Althaus et al. (2007) and Chabrier et al. (2000) do have $\approx 1.0\,M_\odot$ models go below 4000 K (note that the models in Althaus et al. 2007 are primarily O/Ne rather than C/O). However, we believe the $T_{\rm eff}$ upper limits to be more robust, as they do tend to agree between different calculations.

While extreme, the companion to PSR J2222 may not be especially unique. Similar ultra-cool WDs are presumably present in globular clusters and in the field even if they are often too faint to identify on their own. Individual ultra-cool WDs can be identified but only if very nearby, like the two objects in Kilic et al. (2012) at ≈ 30 pc. If we correct roughly for the different progenitor masses between the Kilic et al. (2012) systems and PSR J2222 (Kalirai et al. 2008) and use a Salpeter (1955) initial mass function, we would estimate ≈ 200 massive WDs of a similar age within 300 pc, which is of the same order as the luminosity function from Rowell (2013, also see Giammichele et al. 2012) extrapolated[16] to $M_{\rm bol} > 19$.

Instead, binary systems are the best way to identify cold WDs (e.g., Parsons et al. 2012), which is effectively the technique used here. However, even in binary systems where we know that a source is present, the systems will often be too distant for good constraints (i.e., PSR J1454−5846 in Figure 5; Jacoby et al. 2006). We still require a fortuitously nearby system for

---

[16] Similarly, Giammichele et al. (2012) have a total WD number density of 4×10^{-3} pc^{-3} and Rowell (2013) say that at most a few percent of WDs are lost off the faint end of the luminosity function.

useful observations. The occurrence of a nearby massive WD like the companion to PSR J2222 is reasonably consistent with expectations based on the observed binary population: there are five pulsar binaries from the ATNF Pulsar Catalog[17] (Manchester et al. 2005) within 300 pc, and the other four have low-mass He WD companions. This 1/5 ratio is similar to that for CO WD compared to He WD companions in the whole ATNF catalog (also see Tauris et al. 2012), and the pulsars' spin-down ages appear to have similar distributions for both companion types.

Finally, we can ask whether an NS is the most likely companion to an ultra-cool WD. Most binaries are assumed to have mass ratios near one (Pinsonneault & Stanek 2006, but see Sana et al. 2012), but a binary composed of two ultra-cool WDs would be just as hard to detect optically as a single object. If the companion were a lower-mass WD or a main-sequence star the binary could be visible, although it would require spectroscopic follow-up to identify the companion and in the absence of *GAIA* this has not been done for the majority of stars within a few hundred pc. So the situation of PSR J2222, with an NS companion, is reasonably plausible as the initial mass ratio would have been close to one and the chances of companion follow-up and identification after discovery of the pulsar are high.

4. CONCLUSIONS

We have determined an accurate mass for the partially recycled pulsar PSR J2222 and its companion; the latter is a value consistent with both an NS and a WD. Despite not finding the companion in a deep optical/near-infrared search, we reject a DNS explanation as the binary system shows evidence of circularization requiring mass transfer after the last supernova. Instead, the companion is likely a high-mass WD. Using the extremely precise distance determination from Deller et al. (2013), we can set a robust limit of $M_R > 19.1$. This implies an very old and cool WD: fainter than all other pulsar companions by a factor of about 100, and fainter than the lower-mass "ultra-cool" WD in the solar neighborhood by a factor of about four. Converting this limit to a temperature depends somewhat on the assumed mass and composition, but we believe an effective temperature limit of $T_{\rm eff} < 3000$ K is a robust upper limit. For such an object to not be older than the Milky Way requires that it have already entered the faster Debye cooling regime, i.e., that it already crystallized (also see Metcalfe et al. 2004; Brassard & Fontaine 2005). Future searches, if they can detect the companion to PSR J2222, will be a unique probe of the very late stages of WD evolution, with a well-determined mass and radius that are not usually available for studies of such objects.

Facilities: GBT, Keck:I (LRIS), Keck:II (NIRC2)

REFERENCES

Ahn, C. P., Alexandroff, R., Allende Prieto, C., et al. 2014, ApJS, 211, 17
Althaus, L. G., García-Berro, E., Isern, J., Córsico, A. H., & Rohrmann, R. D. 2007, A&A, 465, 249
Antoniadis, J., Bassa, C. G., Wex, N., Kramer, M., & Napiwotzki, R. 2011, MNRAS, 412, 580
Antoniadis, J., Freire, P. C. C., Wex, N., et al. 2013, Sci, 340, 448
Antoniadis, J., van Kerkwijk, M. H., Koester, D., et al. 2012, MNRAS, 423, 3316
Astropy Collaboration, Robitaille, T. P., Tollerud, E. J., Greenfield, P., et al. 2013, A&A, 558, A33
Bedin, L. R., Salaris, M., Piotto, G., et al. 2009, ApJ, 697, 965
Bergeron, P. 2001, ApJ, 558, 369
Bergeron, P., & Leggett, S. K. 2002, ApJ, 580, 1070
Bergeron, P., Saumon, D., & Wesemael, F. 1995, ApJ, 443, 764
Bergeron, P., Wesemael, F., Dufour, P., et al. 2011, ApJ, 737, 28
Bertin, E., & Arnouts, S. 1996, A&AS, 117, 393
Bertin, E., Mellier, Y., Radovich, M., et al. 2002, in ASP Conf. Ser. 281, Astronomical Data Analysis Software and Systems XI, ed. D. A. Bohlender, D. Durand, & T. H. Handley (San Francisco, CA: ASP), 228
Bhattacharya, D., & van den Heuvel, E. P. J. 1991, PhR, 203, 1
Boyles, J., Lynch, R. S., Ransom, S. M., et al. 2013, ApJ, 763, 80
Brassard, P., & Fontaine, G. 2005, ApJ, 622, 572
Camilo, F., Lyne, A. G., Manchester, R. N., et al. 2001, ApJL, 548, L187
Catalán, S., Napiwotzki, R., Hodgkin, S., et al. 2013, in ASP Conf. Ser. 469, 18th European White Dwarf Workshop, ed. J. Krzesiń, G. Stachowski, P. Moskalik, & K. Bajan (San Francisco, CA: ASP), 235
Catalán, S., Tremblay, P.-E., Pinfield, D. J., et al. 2012, A&A, 546, L3
Chabrier, G., Brassard, P., Fontaine, G., & Saumon, D. 2000, ApJ, 543, 216
Champion, D. J., Ransom, S. M., Lazarus, P., et al. 2008, Sci, 320, 1309
Clemens, J. C., Crain, J. A., & Anderson, R. 2004, Proc. SPIE, 5492, 331
Cordes, J. M., & Lazio, T. J. W. 2002, astro-ph/0207156
Covey, K. R., Ivezić, Ž., Schlegel, D., et al. 2007, AJ, 134, 2398
Damour, T., & Deruelle, N. 1985, AnIHP, 43, 107
Damour, T., & Deruelle, N. 1986, AnIHP, 44, 263
Deller, A. T., Boyles, J., Lorimer, D. R., et al. 2013, ApJ, 770, 145
Demorest, P. B., Pennucci, T., Ransom, S. M., Roberts, M. S. E., & Hessels, J. W. T. 2010, Natur, 467, 1081
Drimmel, R., Cabrera-Lavers, A., & López-Corredoira, M. 2003, A&A, 409, 205
DuPlain, R., Ransom, S., Demorest, P., et al. 2008, Proc. SPIE, 7019, 70191
Ferdman, R. D., Stairs, I. H., Kramer, M., et al. 2010, ApJ, 711, 764
Ferdman, R. D., Stairs, I. H., Kramer, M., et al. 2013, ApJ, 767, 85
Folkner, W. M., Williams, J. G., & Boggs, D. H. 2009, INPR, 178, C1
Freire, P. C. C., & Tauris, T. M. 2014, MNRAS, 438, L86
Gates, E., Gyuk, G., Harris, H. C., et al. 2004, ApJL, 612, L129
Giammichele, N., Bergeron, P., & Dufour, P. 2012, ApJS, 199, 29

Gianninas, A., Bergeron, P., & Ruiz, M. T. 2011, ApJ, 743, 138
Hansen, B. M. S. 1998, Natur, 394, 860
Hansen, B. M. S., Anderson, J., Brewer, J., et al. 2007, ApJ, 671, 380
Holberg, J. B., & Bergeron, P. 2006, AJ, 132, 1221
Hotan, A. W., van Straten, W., & Manchester, R. N. 2004, PASA, 21, 302
Iben, I., Jr., & Tutukov, A. V. 1985, ApJS, 58, 661
Jacoby, B. A., Chakrabarty, D., van Kerkwijk, M. H., Kulkarni, S. R., & Kaplan, D. L. 2006, ApJL, 640, L183
Kalirai, J. S. 2012, Natur, 486, 90
Kalirai, J. S., Hansen, B. M. S., Kelson, D. D., et al. 2008, ApJ, 676, 594
Kasian, L. E. 2012, PhD thesis, Univ. British Columbia
Kaspi, V. M., Lyne, A. G., Manchester, R. N., et al. 2000, ApJ, 543, 321
Keith, M. J., Kramer, M., Lyne, A. G., et al. 2009, MNRAS, 393, 623
Kilic, M., Thorstensen, J. R., Kowalski, P. M., & Andrews, J. 2012, MNRAS, 423, L132
Kim, C., Kalogera, V., & Lorimer, D. R. 2003, ApJ, 584, 985
Kiziltan, B., Kottas, A., De Yoreo, M., & Thorsett, S. E. 2013, ApJ, 778, 66
Koester, D., & Reimers, D. 1996, A&A, 313, 810
Kowalski, P. M., & Saumon, D. 2006, ApJL, 651, L137
Lang, D., Hogg, D. W., Mierle, K., Blanton, M., & Roweis, S. 2010, AJ, 139, 1782
Lattimer, J. M. 2012, ARNPS, 62, 485
Lazarus, P., Tauris, T. M., Knispel, B., et al. 2014, MNRAS, 437, 1485
Lorimer, D. R., & Kramer, M. 2012, Handbook of Pulsar Astronomy (Cambridge: Cambridge University Press)
Lundgren, S. C., Foster, R. S., & Camilo, F. 1996, in ASP Conf. Ser. 105, IAU Colloq. 160: Pulsars: Problems and Progress, ed. S. Johnston, M. A. Walker, & M. Bailes (San Francisco, CA: ASP), 497
Lynch, R. S., Freire, P. C. C., Ransom, S. M., & Jacoby, B. A. 2012, ApJ, 745, 109
Manchester, R. N., Hobbs, G. B., Teoh, A., & Hobbs, M. 2005, AJ, 129, 1993
Mestel, L., & Ruderman, M. A. 1967, MNRAS, 136, 27
Metcalfe, T. S., Montgomery, M. H., & Kanaan, A. 2004, ApJL, 605, L133
Miyaji, S., Nomoto, K., Yokoi, K., & Sugimoto, D. 1980, PASJ, 32, 303
Montgomery, M. H., Klumpe, E. W., Winget, D. E., & Wood, M. A. 1999, ApJ, 525, 482
Nomoto, K. 1984, ApJ, 277, 791
Oke, J. B., Cohen, J. G., Carr, M., et al. 1995, PASP, 107, 375
Ord, S. M., Bailes, M., & van Straten, W. 2002, MNRAS, 337, 409
Özel, F., Psaltis, D., Narayan, R., & Santos Villarreal, A. 2012, ApJ, 757, 55
Pallanca, C., Lanzoni, B., Dalessandro, E., et al. 2013, ApJ, 773, 127
Parsons, S. G., Gänsicke, B. T., Marsh, T. R., et al. 2012, MNRAS, 426, 1950

Phinney, E. S. 1992, RSPTA, 341, 39
Phinney, E. S., & Kulkarni, S. R. 1994, ARA&A, 32, 591
Pinsonneault, M. H., & Stanek, K. Z. 2006, ApJL, 639, L67
Podsiadlowski, P., Langer, N., Poelarends, A. J. T., et al. 2004, ApJ, 612, 1044
Ransom, S. M., Stairs, I. H., Archibald, A. M., et al. 2014, Natur, 505, 520
Richer, H. B., Anderson, J., Brewer, J., et al. 2006, Sci, 313, 936
Richer, H. B., Goldsbury, R., Heyl, J., et al. 2013, ApJ, 778, 104
Rowell, N. 2013, MNRAS, 434, 1549
Salaris, M., Cassisi, S., Pietrinferni, A., Kowalski, P. M., & Isern, J. 2010, ApJ, 716, 1241
Salpeter, E. E. 1955, ApJ, 121, 161
Sana, H., de Mink, S. E., de Koter, A., et al. 2012, Sci, 337, 444
Schwab, J., Podsiadlowski, P., & Rappaport, S. 2010, ApJ, 719, 722
Shapiro, I. I. 1964, PhRvL, 13, 789
Shklovskii, I. S. 1970, SvA, 13, 562
Stairs, I. H. 2010, in IAU Symp. 261, Relativity in Fundamental Astronomy: Dynamics, Reference Frames, and Data Analysis, ed. S. A. Klioner, P. K. Seidelmann, & M. H. Soffel (Cambridge: Cambridge Univ. Press), 218
Tauris, T. M. 2011, in ASP Conf. Ser. 447, Evolution of Compact Binaries, ed. L. Schmidtobreick, M. R. Schreiber, & C. Tappert (San Francisco, CA: ASP), 285
Tauris, T. M., Langer, N., & Kramer, M. 2011, MNRAS, 416, 2130
Tauris, T. M., Langer, N., & Kramer, M. 2012, MNRAS, 425, 1601
Tauris, T. M., Langer, N., & Kramer, M. 2014, ApJ, 781, L13
Tauris, T. M., & van den Heuvel, E. P. J. 2006, in Formation and Evolution of Compact Stellar X-ray Sources, ed. W. H. G. Lewin & M. van der Klis (Cambridge: Cambridge University Press), 623
Tauris, T. M., van den Heuvel, E. P. J., & Savonije, G. J. 2000, ApJL, 530, L93
Taylor, J. H. 1992, RSPTA, 341, 117
Tremblay, P.-E., Bergeron, P., & Gianninas, A. 2011, ApJ, 730, 128
van Dam, M. A., Bouchez, A. H., Le Mignant, D., et al. 2006, PASP, 118, 310
van den Heuvel, E. P. J. 2004, in ESA Special Publication, Vol. 552, 5th INTEGRAL Workshop on the INTEGRAL Universe, ed. V. Schoenfelder, G. Lichti, & C. Winkler (Noordwijk: ESA), 185
van Dokkum, P. G. 2001, PASP, 113, 1420
van Horn, H. M. 1968, ApJ, 151, 227
van Kerkwijk, M. H., Bassa, C. G., Jacoby, B. A., & Jonker, P. G. 2005, in ASP Conf. Ser. 328, Binary Radio Pulsars, ed. F. A. Rasio & I. H. Stairs (San Fransisco, CA: ASP), 357
van Kerkwijk, M. H., & Kulkarni, S. R. 1999, ApJL, 516, L25
van Leeuwen, J., Kasian, L., Stairs, I. H., et al. 2014, ApJ, submitted
Williams, K. A., Bolte, M., & Koester, D. 2009, ApJ, 693, 355